Exact Diagonalization for Magic-Angle Twisted Bilayer Graphene

Pawel Potasz[ORCID]

Department of Physics, The University of Texas at Austin, Austin, Texas 78712, USA
and Department of Physics, Wroclaw University of Science and Technology, 50-370 Wroclaw, Poland

Ming Xie[ORCID] and A. H. MacDonald[ORCID]

Department of Physics, The University of Texas at Austin, Austin, Texas 78712, USA

We report on finite-size exact-diagonalization calculations in a Hilbert space defined by the continuum-model flat moiré bands of magic angle twisted bilayer graphene. For moiré band filling $3 > |\nu| > 2$, where superconductivity is strongest, we obtain evidence that the ground state is a spin ferromagnet. Near $|\nu| = 3$, we find Chern insulator ground states that have spontaneous spin, valley, and sublattice polarization, and demonstrate that the anisotropy energy in this order-parameter space is strongly band-filling-factor dependent. We emphasize that inclusion of the remote band self-energy is necessary for a reliable description of magic angle twisted bilayer graphene flat band correlations.

Introduction.—Near a magic twist angle, the width of bilayer graphene's low energy moiré bands shrinks [1,2] by an order of magnitude or more, allowing interactions to play a prominent role in shaping electronic properties. The flat bands form an octet that is the direct product of twofold spin, valley, and band or sublattice degrees of freedom and closely analogous to the spin, valley, or layer octet of Bernal bilayer graphene [3–6]. The recent discovery of superconductivity and interaction-induced Chern and trivial insulator states [7–25] in magic-angle twisted bilayer graphene (MATBG) has motivated ongoing theoretical work [26–82], from which it is already clear that, although MATBG states share properties with doped and undoped Mott insulators in conventional crystals, they also have a relationship to integer and fractional quantum Hall states [45,61,62].

Progress in understanding competitions between different low energy states and the sensitivity of the ground state properties to particular model parameters has been achieved using numerical mean-field theory [11,24,31,43,44,46,48, 51,69], and beyond, using exact diagonalization [39,75,79], quantum Monte Carlo [32,34,80] and density matrix renormalization group methods [50,51,79,81,82], and using both Hubbard-like lattice [14,15,25–27,31–35,37–39,41, 52,61,62,78,80] and continuum models [11,24,43,44, 46,48,51,69–75,79,81,82]. In this Letter we use exact diagonalization to describe correlations within flat bands that are identified by solving the single-particle problem [2] exactly. The use of numerical flat bands in place of approximate Wannier orbitals has the advantage that we account accurately for crucial changes in the charge distribution of flat band wave functions as a function of moiré Brillouin-zone momentum. We use a systematic approach that accounts fully for self-energies from remote bands, which play a key role, to make further progress. Because the MATBG octet enlarges finite Hilbert space sizes far beyond those of spinful single-band models, we are forced to restrict our attention primarily to flat band filling factors with $|\nu| \geq 2$; fortunately much of the strong correlation physics seen experimentally occurs in this filling factor regime.

Our calculations confirm [19–21,24] that spin, valley, and sublattice polarization is common in both insulating and metallic states, demonstrate that the anisotropy energy associated with these generalized ferromagnetic orders is strongly filling factor dependent, and provide evidence for spin-polarized ground states for $|\nu| \in (2, 3)$—the range of filling factor that supports the strongest superconductivity. This picture is revealed in exact diagonalization (ED) finite-size system results by signatures of macroscopic quantum tunneling. Our main results are presented in Fig. 1 where panel (a) provides evidence that ground states are maximally spin-polarized for $|\nu| \in (2, 3)$, but valley-polarized only near $|\nu| = 3$. Figure 1(b) shows that the ground state at $|\nu| = 3$ is a spin and valley polarized doublet formed by states with opposite senses of spontaneous sublattice polarization. These states are known to be Chern insulators and are accurately approximated by Hartree-Fock theory. The ground state of the system with one charge added to (or removed from) the $|\nu| = 3$ ground state [Fig. 1(c)] is still fully spin polarized but completely loses its K, K' valley polarization. As shown in Fig. 1(d) these states nevertheless have precisely integer occupation numbers for all momenta, but only when summed over valleys. We conclude that the states with added and removed charge have easy-plane valley order; we attribute the sudden change in anisotropy
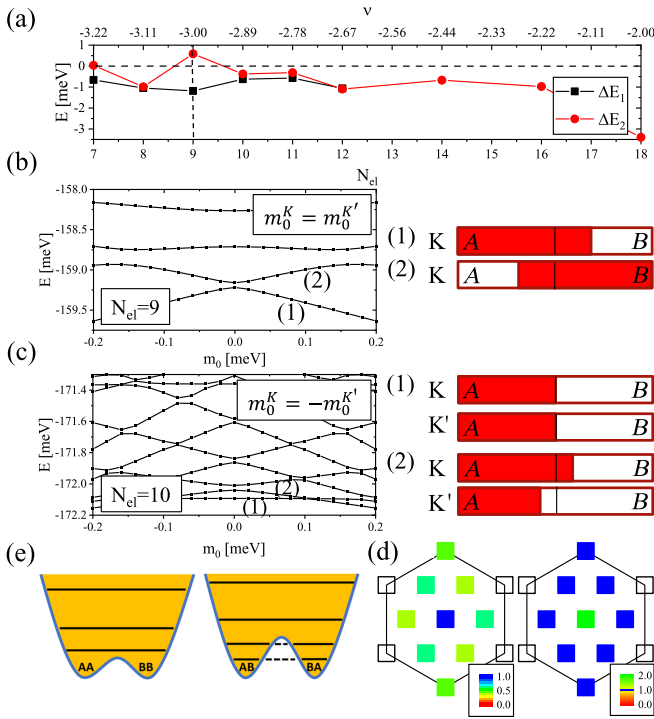
FIG. 1. Spin, valley, and sublattice order vs electron number N_{el} in finite-size MATBG with $M = 9$ moiré unit cells: (a) $\Delta E_1 = E_{min}(S_{max}) - E_{min}(S < S_{max})$ (meV/unit cell), where $S = S_K + S_{K'}$ is total spin and $S_{max} = N_{el}/2$ is its maximal value. $\Delta E_2 = E_{min}(P_v = 0) - E_{min}(P_v = 1)$ where $P_v = |N_K - N_{K'}|/(N_K + N_{K'})$. (b) Response of the ground state energy of the valley polarized state at $|\nu| = 3$ to an external field that couples to sublattice polarization. (c) Response of low energy states to a valley-odd sublattice field at $N_{el} = 10$. The right panels in (b) and (c) schematically illustrate the sublattice polarizations induced in states (1) and (2) by the corresponding fields. (d) Ground state momentum space occupation numbers projected to valley K (left), and traced over valley (right) at $N_{el} = 10$. (e) Schematic illustration of macroscopic quantum tunneling of the sublattice pseudospin collective coordinate, based on $N_{el} = 10$ ED results. The ground state (1)(left) has the same sense of sublattice polarization in the two valleys, and at this system size, strong hybridization between the sublattice polarization states labeled AA and BB, where the first letter corresponds to valley K and the second to valley K'. The first excited state (2) (right) has opposite sense of sublattice polarization in opposite valleys (AB) and (BA), and much weaker hybridization between the two degenerate states at this system size.

to the strong band and sublattice dependence of the single-particle Hamiltonian at momenta near the γ point in the moiré Brillouin zone. The sublattice polarization-properties [Fig. 1(e)] of the ground states near $|\nu| = 3$, discussed further below, are revealed by the responses to sublattice and valley dependent potentials illustrated in Figs. 1(b) and 1(c).

Flat band projected exact diagonalization.—Because of large Dirac velocities, the electronic density of states of an isolated neutral graphene sheet has a minimum at neutrality

and is small over a broad energy range, allowing interaction effects to be described perturbatively. When magic-angle moiré bands [2] are formed, strong electronic correlations emerge and perturbative analyses are less reliable. The ED of the Hamiltonian is a powerful nonperturbative method to study strong correlations, but, because the many-body Hilbert space grows exponentially with system size, it is practical only when the single-particle Hamiltonian can be truncated to a reasonably small dimension, typically with at most several tens of single-particle states. In MATBG the spectral isolation of the eight flat bands of interest (flat conduction and valence bands for each of four spin or valley flavors) motivates projection to an occupation number subspace in which all remote valence bands in graphene's negative-energy sea are fully occupied, all remote conduction bands are empty, and occupation numbers are allowed to fluctuate only within the flat bands. This strategy leads to a low-energy effective Hamiltonian that acts entirely in the flat-band Hilbert space:

$$H_{\text{eff}} = \sum_{i',i} [\epsilon_i \delta_{i',i} + \Sigma_{i',i}] c_{i'}^\dagger c_i$$
$$+ \frac{1}{2} \sum_{i',i,j',j} \langle i', j'|V|i, j\rangle c_{i'}^\dagger c_{j'}^\dagger c_j c_i, \tag{1}$$

where $\langle i', j'|V|i, j\rangle$ is a two-body Coulomb interaction matrix element, i', i, j', j label flat band states, ϵ_i is an eigenvalue of the single-particle twisted-bilayer graphene Hamiltonian [2] including the interlayer tunneling contribution that is responsible for flat band formation, and

$$\Sigma_{i',i} = \sum_v [\langle i', v|V|i, v\rangle - \langle i', v|V|v, i\rangle]$$
$$- \sum_{\bar{v}} [\langle i', \bar{v}|V|i, \bar{v}\rangle - \langle i', \bar{v}|V|\bar{v}, i\rangle], \tag{2}$$

which we refer to the remote band self energy, accounts for Hartree and exchange interactions with states v in the frozen negative energy sea. In Eq. (2) the sum over $\bar{v}$ in the regularization term is over the frozen valence bands of a neutral bilayer with no-interlayer tunneling [43]. As we shall emphasize, the remote band self-energy plays an essential role in MATBG physics and unlike in the related case of Landau level physics, cannot be neglected. Its importance derives from the fact that flat valence band wave functions have strongly momentum-dependent spatial distributions across the moiré unit cell, even when averaged over the full band [36,42]. This issue is solved by appropriately renormalizing the flat bands by adding self-energies from the remote valence bands. Both Hartree and Fock terms are essential when considering the physics away from the neutrality point (fully filled flat valence band) in effective Hamiltonians projected to flat band subspace. This self-energy accounts for leading-order interactions between flat and remote bands, and includes

exchange interactions that enhance intersubband layer coupling as emphasized in a recent perturbative renormalization group calculation by Kang and Vafek [76]. At higher order, remote band polarization will screen the Coulomb interaction in Eq. (1), among other less understood effects. We partially account for these screening effect [77] by allowing the (in general q dependent) dielectric function used in constructing the Coulomb matrix elements to be larger than the value that would be expected on the basis of dielectric and gate screening alone.

The remote band self-energy reshapes the bands principally by shifting energies near γ upward, relative to those near κ, κ'. The relative shifts occur primarily because the Hartree potential from the remote bands is attractive near the AA positions where states near γ have less weight [36,42,43]. The sharp contrast between the conduction and valence band widths in these empty-band dispersions does not imply strong particle-hole asymmetry. Indeed the model we will study is very nearly particle-hole symmetric, and the relative widths of the bands is reversed when we describe flat band states in terms of interacting holes instead of interacting electrons [83]. Instead, the upward shift at γ works in concert with weaker electron-electron repulsion matrix elements for states near γ [83] that reduce their Coulomb energy penalty as the flat bands are filled. The ED results in this work were calculated at twist angle $\theta = 1.1$, interaction strength parameter $\epsilon^{-1} = 0.05$, for the $M = 9$ moiré unit cells system, which is sufficiently large to capture the important distinction between states near γ and those in the rest of the Brillouin zone. Unlike the model we study, experimental samples do exhibit clear particle-hole asymmetry. For example, the Chern insulator states we discuss below tend to be more prominent at positive than at negative filling factors. The asymmetry is thought [44] to be due to nonlocal corrections to the interlayer tunneling model we employ. The relationship of our findings to experiment is addressed more fully in the discussion section below.

The many-body Hamiltonian separates into decoupled blocks labeled by the number of electrons in each valley N_K and $N_{K'}$, valley-dependent total (S_K and $S_{K'}$) and azimuthal spin (S_K^z and $S_{K'}^z$) quantum numbers, and total crystal momentum (K_x, K_y). The separate spin quantum numbers for the two valleys apply because the model is invariant under independent valley-dependent spin rotations.

Numerical results.—Our first important result is related to the regime in which $|\nu| \in (2, 3)$, where the ground state is commonly observed to have two occupied flavors. (Our ED calculations have little access to the $|\nu| < 2$ region of filling factor, which fortunately are of lesser interest because they tend to have relatively well understood Fermi liquid ground state with no broken symmetries [14,15,44].) A key issue is whether these states are fully spin polarized, or fully valley polarized, or in some other more complicated two-flavor state. Our ED calculations do
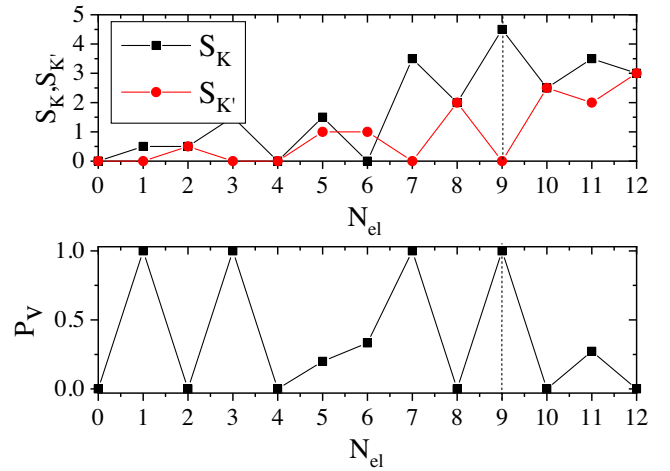

FIG. 2. Ground state spin and valley quantum numbers as a function of electron number N_{el}. Top: total spin S_K and $S_{K'}$ in each valley. Bottom: valley polarization P_v. Integer band filling $\nu = -3$ occurs at $N_{el} = 9$ highlighted by a dashed line. $S = S_K + S_{K'}$ is total spin.

not have access to the full Hilbert space across the entire $|\nu| \in (2, 3)$ interval, which corresponds to the $N_{el} \in [10, 18]$ in our flat-band projected ED calculation. For $N_{el} = 10$, 11, 12 full Hilbert space calculations confirm that the ground state is maximally spin-polarized, as illustrated in Fig. 2. For larger N_{el} we can show that the fully spin-polarized state is lower in energy than the corresponding fully valley-polarized state. Some of these conclusions rest on extrapolations from calculations performed in a selected subspace of the full ED Hilbert space, as explained in the Supplemental Material [83]. The conclusion that the ground state is fully spin polarized helps constrain and simplify potential theories of superconductivity.

For $N_{el} = 9$ ($|\nu| = 3$), we are able to fully explore nearly all subspaces, including all with particles distributed over three flavors, and subspaces with particles distributed over four flavors provided one of the flavors is filled by at least five particles. We find that the ground state is fully spin and valley polarized, and well approximated by a single Slater determinant. For example, we find that the maximum deviation from unit momentum-state occupation across the Brillouin zone is 0.04. The ground state appears as a quartet with nearly degenerate doublets for each sense of valley polarization. By studying the response of this doublet to a sublattice dependent potential $m_0 \sigma_z$, where σ_z acts on the sublattice degree-of-freedom in both layers, we see that for a given valley polarization the doublet is formed by states with opposite sublattice polarizations and that there is observable hybridization between these states. It is known from Hartree-Fock theory that these states are Chern insulators with Chern number magnitudes $|C| = 1$ and signs determined by the sign of the product of the valley and sublattice polarization. In Refs. [47,48] the two

states with the same Chern number are described by a σ model in which only the orientation of the corresponding pseudospin is retained as a relevant degree of freedom. The Chern insulator at $|\nu| = 3$ [45,46,64,65] can be viewed as a simple ferromagnet formed from these pseudospins. From Fig. 1(b) we conclude that $\langle \sigma_z \rangle \sim 2.25$, implying that $P_{\text{sub}} = \langle \sigma_z \rangle / N_{\text{el}} \sim 0.25$, in agreements with previous Hartree-Fock results [43,46], and that the Hamiltonian matrix element for collective tunneling between states with opposite senses of spontaneous sublattice polarization (which is expected to fall exponentially with system size) is ∼0.058 meV for $N_{\text{el}} = M = 9$ and (based on a separate calculation) ∼0.0094 meV for $N_{\text{el}} = M = 16$ calculation.

Easy-plane valley anisotropy.—In Figs. 1(c) and 2 we see that valley polarization is completely lost when we add or remove one electron from the $N_{\text{el}} = 9$ valley and spin polarized ferromagnet. We attribute this behavior to the strong band splitting at γ, which has an outsized influence on valley anisotropy by suppressing the band-mixing degree of freedom. An important element of our interpretation is the observation that our system has only U(1) and not SU(2) valley symmetry. In the language of magnetism our system has uniaxial valley anisotropy, which allows easy axis or easy-plane valley magnetism. Our conclusion that the state at γ plays a crucial role is supported by the property that the excitation spectra at $N = 8$, where the γ state is empty, and at $N = 10$, where the γ state is doubly occupied, are nearly identical. Our calculations confirm that easy axis sublattice order is present for both easy-axis and easy-plane valley anisotropy, with four degenerate classical states distinguished by the sublattice polarization of K and K' valley components in the easy plane case. The ground state responds most strongly to sublattice potentials that are identical in the two valleys, demonstrating AA or BB sublattice polarizations (see [83]). These two classical states should have identical energies, and we conclude from the ED spectra that the tunneling between them is large at this system size. We associate the excited state doublets in Fig. 1(c) with AB and BA sublattice polarizaiton for valleys KK'. This interpretation is supported by strong response to valley-odd sublattice potentials. Our ED results demonstrate that the many-particle tunneling matrix element between these sublattice states is greatly reduced compared to tunneling between degenerate AA and BB states. In this case the ED spectra exhibit resonant tunneling not only between ground states, but also between excited states of the isolated AB and BA sectors.

Discussion.—Our calculations show that MATBG ground state energies are generally speaking well approximated by unrestricted Hartree-Fock approximations that allow spin, valley, and sublattice symmetries to be broken. In the top panel of Fig. 3 we show the dependence of the correlation energy on electron number in the subspace with full spin and valley flavor polarization over the full range of available filling factor for that flavor between $\nu_f = -1$ and
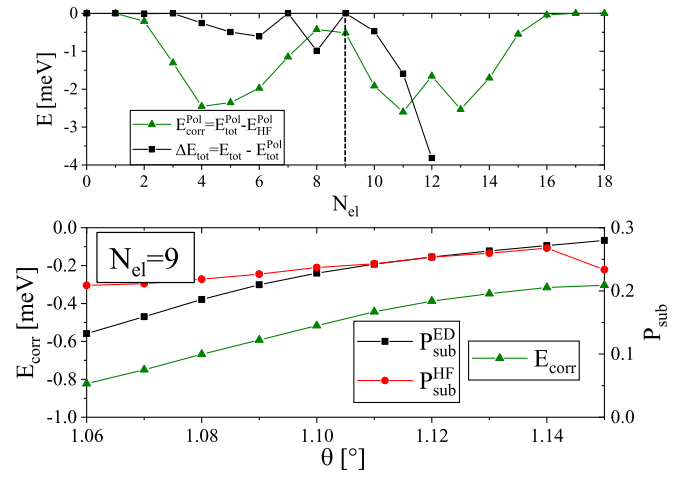

FIG. 3. The correlation energy per moiré period as a function of filling factor (top) and as a function of the twist angle for $N_{\text{el}} = 9$ together with corresponding sublattice polarizations (bottom). Within this range of angles, both exact diagonalization and Hartree-Fock calculations predict full flavor polarization. Top: the green triangles correspond to one flavor full-spin-polarization calculations and $E_{\text{corr}}^{\text{Pol}} = E_{\text{tot}}^{\text{Pol}} - E_{\text{HF}}^{\text{Pol}}$, where $E_{\text{tot}}^{\text{Pol}}$ is the ground state energy from exact diagonalization calculations and $E_{\text{HF}}^{\text{Pol}}$ is the mean-field energy from self-consistent Hartree-Fock calculations. The black squares show to the energy difference between the ground state energy and the lowest energy state in the full flavor polarization sector. The black dashed line marks the filling factor $\nu = -3$. Bottom: the twist angle dependence at $N_{\text{el}} = 9$ with green triangles for the correlation energy and black squares and red circles for ED and HF sublattice polarizations.

$\nu_f = 1$. The correlation energy, defined as the difference between the ED ground state energy and the minimum energy single-Slater determinant, vanishes when the orbital doublet is empty ($\nu_f = -1$) and full ($\nu_f = 1$), and also when it reaches an extremely small value in the insulating state at $\nu_f = 0$. These results suggest insulating states at all integer filling factors with a band filling per flavor equal to -1, 0, or 1 are accurately rendered by Hartree-Fock calculations, even when symmetry is broken by choosing different band filling factors for different flavors. For a given total integer filling factor a variety of different states, characterized by different flavor-dependent filling factors and senses of sublattice polarization, are expected to compete closely in energy. The states have different total Chern numbers with $|C| = 1$ for $|\nu| = 3$, 0, or 2 for $|\nu| = 2$, 1, or 3 for $|\nu| = 1$, and 0, 2, or 4 for $\nu = 0$. (The $|\nu| = 1$ and $|\nu| = 0$ cases are outside of the reach of ED.) In Fig. 3 we see that the correlation energy is larger away from integer filling factors. We expect that this trend will be stronger in sectors with less flavor polarization, and that Hartree-Fock calculation therefore overestimates the tendency to break flavor symmetries. Insulating states at $|\nu| = 1$ will therefore compete with metallic states with no broken flavor symmetries that have much larger correlation energies.

The difference in energy between the true ground state and the ground state in the fully polarized sector increases quickly for $N_{el} > 9$, showing that the energy cost of valley polarization quickly increases.

The appearance of insulating states at integer filling factors depends on screening environment, twist angle, and band structure details that we have not fully explored here. For example in the bottom panel of Fig. 3 we illustrate how the correlation energy of the $\nu = -3$ Chern insulator state depends on twist angle. As expected the correlation energy is reduced as the twist angle increases relative to the magic angle. Surprisingly though, the sublattice polarization increases and is more accurately estimated by Hartree-Fock calculations as twist angle increases [43]. Evidently the physics responsible for the broken symmetries is basically that of exchange interactions, which are captured by Hartree-Fock calculations, with correlations working against order. While finite size effects are present in all ED calculations, a direct comparison with Hartree-Fock results for the same system size (Fig. 3) and results extrapolated to the thermodynamic limit shown in the Supplemental Material [83] confirm this conclusion. Like the twist angle θ, the screening parameter ϵ used in our calculations influences quantitative conclusions. Interactions in the flat bands of MATBG are screened by the surrounding hexagonal boron nitride dielectric, by the nearby electrical gates, and by transitions between the flat and remote bands [77]. Strictly speaking, the latter two effects yield wave-vector-dependent contributions to the dielectric constant with gates dominating in importance at small wave vectors and screening within the bilayer dominating a larger wave vectors.

---

[1] E. Suarez Morell, J. D. Correa, P. Vargas, M. Pacheco, and Z. Barticevic, Phys. Rev. B **82**, 121407(R) (2010).

[2] R. Bistritzer and A. H. MacDonald, Proc. Natl. Acad. Sci. U.S.A. **108**, 12233 (2011).

[3] Maxim Kharitonov, Phys. Rev. B **86**, 195435 (2012).

[4] F. Zhang, J. Jung, G. A. Fiete, Q. Niu, and A. H. MacDonald, Phys. Rev. Lett. **106**, 156801 (2011).

[5] A. H. MacDonald1, J. Jung, and F. Zhang, Phys. Scr. **T146**, 014012 (2012).

[6] Y. Barlas, R. Cote, K. Nomura, and A. H. MacDonald, Phys. Rev. Lett. **101**, 097601 (2008).

[7] K. Kim, A. DaSilva, S. Huang, B. Fallahazad, S. Larentis, T. Taniguchi, K. Watanabe, B. J. LeRoy, A. H. MacDonald, and E. Tutuc, Proc. Natl. Acad. Sci. U.S.A. **114**, 3364 (2017).

[8] Y. Cao, V. Fatemi, A. Demir, S. Fang, S. L. Tomarken, J. Y. Luo, J. D. Sanchez-Yamagishi, K. Watanabe, T. Taniguchi, E. Kaxiras, R. C. Ashoori, and P. Jarillo-Herrero, Nature (London) **556**, 80 (2018).

[9] Y. Cao, V. Fatemi, S. Fang, K. Watanabe, T. Taniguchi, E. Kaxiras, and P. Jarillo-Herrero, Nature (London) **556**, 43 (2018).

[10] M. Yankowitz, S. Chen, H. Polshyn, K. Watanabe, T. Taniguchi, D. Graf, A. F. Young, and C. R. Dean, Science **363**, 1059 (2019).

[11] X. Lu, P. Stepanov, W. Yang, M. Xie, M. Ali Aamir, I. Das, C. Urgell, K. Watanabe, T. Taniguchi, G. Zhang, A. Bachtold, A. H. MacDonald, and D. K. Efetov, Nature (London) **574**, 653 (2019).

[12] A. Uri, S. Grover, Y. Cao, J. A. Crosse, K. Bagani, D. Rodan-Legrain, Y. Myasoedov, K. Watanabe, T. Taniguchi, P. Moon, M. Koshino, P. Jarillo-Herrero, and E. Zeldov, Nature (London) **581**, 47 (2020).

[13] L. Balents, C. R. Dean, D. K. Efetov, and A. F. Young, Nat. Phys. **16**, 725 (2020).

[14] D. Wong, K. P. Nuckolls, M. Oh, B. Lian, Y. Xie, S. Jeon, K. Watanabe, T. Taniguchi, B. A. Bernevig, and A. Yazdani, Nature (London) **582**, 198 (2020).

[15] U. Zondiner, A. Rozen, D. Rodan-Legrain, Y. Cao, R. Queiroz, T. Taniguchi, K. Watanabe, Y. Oreg, F. von Oppen, Ady Stern, E. Berg, P. Jarillo-Herrero, and S. Ilani, Nature (London) **582**, 203 (2020).

[16] A. L. Sharpe, E. J. Fox, A. W. Barnard, J. Finney, K. Watanabe, T. Taniguchi, M. A. Kastner, and D. Goldhaber-Gordon, Science **365**, 605 (2019).

[17] M. Serlin, C. L. Tschirhart, H. Polshyn, Y. Zhang, J. Zhu, K. Watanabe, T. Taniguchi, L. Balents, and A. F. Young, Science **367**, 900 (2020).

[18] P. Stepanov, I. Das, X. Lu, A. Fahimniya, K. Watanabe, T. Taniguchi, F. H. L. Koppens, J. Lischner, L. Levitov, and D. K. Efetov, Nature (London) **583**, 375 (2020).

[19] S. Wu, Z. Zhang, K. Watanabe, T. Taniguchi, and E. Y. Andrei, Nat. Mater. **20**, 488 (2021).

[20] I. Das, X. Lu, J. Herzog-Arbeitman, Z.-D. Song, K. Watanabe, T. Taniguchi, B. A. Bernevig, and D. K. Efetov, Nat. Phys. **17**, 710 (2021).

[21] J. M. Park, Y. Cao, K. Watanabe, T. Taniguchi, and P. Jarillo-Herrero, Nature (London) **592**, 43 (2021).

[22] H. S. Arora, R. Polski, Y. Zhang, A. Thomson, Y. Choi, H. Kim, Z. Lin, I. Z. Wilson, X. Xu, J.-H. Chu, K.Watanabe, T. Taniguchi, J. Alicea, and S. Nadj-Perge, Nature (London) **583**, 379 (2020).

[23] Y. Cao, D. Rodan-Legrain, J. Min Park, F. N. Yuan, K. Watanabe, T. Taniguchi, R. M. Fernandes, L. Fu, and P. Jarillo-Herrero, Science **372**, 264 (2021).

[24] P. Stepanov, M. Xie, T. Taniguchi, K. Watanabe, X. Lu, A. H. MacDonald, B. Andrei Bernevig, and D. K. Efetov, arXiv:2012.15126.

[25] A. Rozen, J. M. Park, U. Zondiner, Y. Cao, D. Rodan-Legrain, T. Taniguchi, K. Watanabe, Y. Oreg, Ady Stern, E. Berg, P. Jarillo-Herrero, and S. Ilani, Nature (London) **592**, 214 (2021).

[26] N. F. Q. Yuan and L. Fu, Phys. Rev. B **98**, 045103 (2018).

[27] H. C. Po, L. Zou, A. Vishwanath, and T. Senthil, Phys. Rev. X **8**, 031089 (2018).

[28] H. Guo, X. Zhu, S. Feng, and R. T. Scalettar, Phys. Rev. B **97**, 235453 (2018).

[29] B. Padhi, C. Setty, and P. W. Phillips, Nano Lett. **18**, 6175 (2018).

[30] V. Y. Irkhin and Y. N. Skryabin, JETP Lett. **107**, 651 (2018).

[31] J. F. Dodaro, S. A. Kivelson, Y. Schattner, X.-Q. Sun, and C. Wang, Phys. Rev. B **98**, 075154 (2018).

[32] T. Huang, L. Zhang, and T. Ma, Sci. Bull. **64**, 310 (2019).

[33] C.-C. Liu, L.-D. Zhang, W.-Q. Chen, and F. Yang, Phys. Rev. Lett. **121**, 217001 (2018).

[34] X. Y. Xu, K. T. Law, and P. A. Lee, Phys. Rev. B **98**, 121406(R) (2018).

[35] J. Kang and O. Vafek, Phys. Rev. X **8**, 031088 (2018).

[36] L. Rademaker and P. Mellado, Phys. Rev. B **98**, 235158 (2018).

[37] M. Koshino, N. F. Q. Yuan, T. Koretsune, M. Ochi, K. Kuroki, and L. Fu, Phys. Rev. X **8**, 031087 (2018).

[38] J. M. Pizarro, M. J. Calderon, and E. Bascones, J. Phys. Commun. **3**, 035024 (2019).

[39] M. Ochi, M. Koshino, and K. Kuroki, Phys. Rev. B **98**, 081102(R) (2018).

[40] H. Isobe, N. F. Q. Yuan, and L. Fu, Phys. Rev. X **8**, 041041 (2018).

[41] A. Thomson, S. Chatterjee, S. Sachdev, and M. S. Scheurer, Phys. Rev. B **98**, 075109 (2018).

[42] F. Guinea and N. R. Walet, Proc. Natl. Acad. Sci. U.S.A. **115**, 13174 (2018).

[43] Ming Xie and Allan H. MacDonald, Phys. Rev. Lett. **124**, 097601 (2020).

[44] Ming Xie and Allan H. MacDonald, arXiv:2010.07928v1.

[45] N. Bultinck, S. Chatterjee, and M. P. Zaletel, Phys. Rev. Lett. **124**, 166601 (2020).

[46] N. Bultinck, E. Khalaf, S. Liu, S. Chatterjee, A. Vishwanath, and M. P. Zaletel, Phys. Rev. X **10**, 031034 (2020).

[47] E. Khalaf, S. Chatterjee, N. Bultinck, M. P. Zaletel, and A. Vishwanath, Sci. Adv. **7**, eabf5299 (2021).

[48] E. Khalaf, N. Bultinck, A. Vishwanath, and M. P. Zaletel, arXiv:2009.14827.

[49] S. Chatterjee, N. Bultinck, and M. P. Zaletel, Phys. Rev. B **101**, 165141 (2020).

[50] S. Chatterjee, M. Ippoliti, and M. P. Zaletel, arXiv:2010.01144.

[51] D. E. Parker, T. Soejima, J. Hauschild, M. P. Zaletel, and Nick Bultinck, Phys. Rev. Lett. **127**, 027601 (2021).

[52] C. Xu and L. Balents, Phys. Rev. Lett. **121**, 087001 (2018).

[53] F. Wu, A. H. MacDonald, and I. Martin, Phys. Rev. Lett. **121**, 257001 (2018).

[54] B. Roy and V. Juricic, Phys. Rev. B **99**, 121407(R) (2019).

[55] S. Ray, J. Jung, and T. Das, Phys. Rev. B **99**, 134515 (2019).

[56] T. J. Peltonen, R. Ojajarvi, and T. T. Heikkila, Phys. Rev. B **98**, 220504(R) (2018).

[57] Y.-Z. You and A. Vishwanath, Quantum Mater. **4**, 16 (2019).

[58] X.-C. Wu, K. A. Pawlak, C.-M. Jian, and C. Xu, arXiv:1805.06906.

[59] M. Fidrysiak, M. Zegrodnik, and J. Spalek, Phys. Rev. B **98**, 085436 (2018).

[60] J. M. B. Lopes dos Santos, N. M. R. Peres, and A. H. Castro Neto, Phys. Rev. Lett. **99**, 256802 (2007).

[61] H. C. Po, H. Watanabe, and A. Vishwanath, Phys. Rev. Lett. **121**, 126402 (2018).

[62] H. C. Po, L. Zou, T. Senthil, and A. Vishwanath, Phys. Rev. B **99**, 195455 (2019).

[63] G. Tarnopolsky, A. J. Kruchkov, and A. Vishwanath, Phys. Rev. Lett. **122**, 106405 (2019).

[64] J. Liu, J. Liu, and X. Dai, Phys. Rev. B **99**, 155415 (2019).

[65] Y.-H. Zhang, D. Mao, Y. Cao, P. Jarillo-Herrero, and T. Senthil, Phys. Rev. B **99**, 075127 (2019).

[66] G. W. Semenoff, Phys. Scr. **T146**, 014016 (2012).

[67] J. Jung, A. Raoux, Z. Qiao, and A. H. MacDonald, Phys. Rev. B **89**, 205414 (2014).

[68] Y. Saito, J. Ge, K. Watanabe, T. Taniguchi, and A. F. Young, Nat. Phys. **16**, 926 (2020).

[69] A. Kumar, M. Xie, and A. H. MacDonald, Phys. Rev. B **104**, 035119 (2021).

[70] B. A. Bernevig, Z. D. Song, N. Regnault, and B. Lian, Phys. Rev. B **103**, 205411 (2021).

[71] Z.-D. Song, B. Lian, N. Regnault, and B. A. Bernevig, Phys. Rev. B **103**, 205412 (2021).

[72] B. A. Bernevig, Z. D. Song, N. Regnault, and B. Lian, Phys. Rev. B **103**, 205413 (2021).

[73] B. Lian, Z. D. Song, N. Regnault, D. K. Efetov, A. Yazdani, and B. A. Bernevig, Phys. Rev. B **103**, 205414 (2021).

[74] B. A. Bernevig, B. Lian, A. Cowsik, F. Xie, N. Regnault, and Z. D. Song, Phys. Rev. B **103**, 205415 (2021).

[75] F. Xie, A. Cowsik, Z. D. Song, B. Lian, B. A. Bernevig, and N. Regnault, Phys. Rev. B **103**, 205416 (2021).

[76] Oskar Vafek and Jian Kang, Phys. Rev. Lett. **125**, 257602 (2020).

[77] J. M. Pizarro, M. Rosner, R. Thomale, R. Valenti, and T. O. Wehling, Phys. Rev. B **100**, 161102(R) (2019).

[78] Jian Kang and Oskar Vafek, Phys. Rev. Lett. **122**, 246401 (2019).

[79] C. Repellin, Z. Dong, Y.-H. Zhang, and T. Senthil, Phys. Rev. Lett. **124**, 187601 (2020).

[80] Y. Da Liao, Z. Y. Meng, and X. Y. Xu, Phys. Rev. Lett. **123**, 157601 (2019).

[81] T. Soejima, D. E. Parker, N. Bultinck, J. Hauschild, and M. P. Zaletel, Phys. Rev. B **102**, 205111 (2020).

[82] J. Kang and O. Vafek, Phys. Rev. B **102**, 035161 (2020).

[83] See the Supplemental Materials at http://link.aps.org/supplemental/10.1103/PhysRevLett.127.147203 for additional filling factor dependent results.